University of Massachusetts - Amherst
ScholarWorks@UMass Amherst

Astronomy Department Faculty Publication Series | Astronomy

2007

The Galactic Central Diffuse X-Ray Enhancement: A Differential Absorption/Emission Analysis

Y Yao

QD Wang
University of Massachusetts - Amherst, wqd@astro.umass.edu

Follow this and additional works at: http://scholarworks.umass.edu/astro_faculty_pubs

 Part of the Astrophysics and Astronomy Commons

Yao, Y and Wang, QD, "The Galactic Central Diffuse X-Ray Enhancement: A Differential Absorption/Emission Analysis" (2007). *Astronomy Department Faculty Publication Series.* Paper 1088.
http://scholarworks.umass.edu/astro_faculty_pubs/1088

This Article is brought to you for free and open access by the Astronomy at ScholarWorks@UMass Amherst. It has been accepted for inclusion in Astronomy Department Faculty Publication Series by an authorized administrator of ScholarWorks@UMass Amherst. For more information, please contact scholarworks@library.umass.edu.

Accepted for publication in the Astrophysical Journal
Preprint typeset using LaTeX style emulateapj v. 10/09/06

arXiv:0705.2772v2 [astro-ph] 26 Jul 2007

THE GALACTIC CENTRAL DIFFUSE X-RAY ENHANCEMENT: A DIFFERENTIAL ABSORPTION/EMISSION ANALYSIS

YANGSEN YAO[1] AND Q. DANIEL. WANG[2]

Accepted for publication in the Astrophysical Journal

ABSTRACT

The soft X-ray background shows a general enhancement toward the inner region of the Galaxy. But whether this enhancement is a local feature (e.g., a superbubble within a distance of $\lesssim$200 pc) and/or a phenomenon related to energetic outflows from the Galactic center/bulge remains unclear. Here we report a comparative X-ray emission and absorption study of diffuse hot gas along the sight lines toward 3C 273 and Mrk 421, on and off the enhancement, but at similar Galactic latitudes. The diffuse 3/4-keV emission intensity, as estimated from the *ROSAT* All Sky Survey, is about 3 times higher toward 3C 273 than toward Mrk 421. Based on archival *Chandra* grating observations of these two AGNs, we detect X-ray absorption lines (e.g., O VII Kα, Kβ, and O VIII Kα transitions at $z \sim 0$) and find that the mean hot gas thermal and kinematic properties along the two sight lines are significantly different. By subtracting the foreground and background contribution, as determined along the Mrk 421 sight line, we isolate the net X-ray absorption and emission produced by the hot gas associated with the enhancement in the direction of 3C 273. From a joint analysis of these differential data sets, we obtain the temperature, dispersion velocity, and hydrogen column density as $2.0(1.6, 2.3) \times 10^6$ K, 216(104, 480) km s^{-1}, and $2.2(1.4, 4.1) \times 10^{19}$ cm^{-2}, respectively (90% confidence intervals), assuming that the gas is approximately isothermal, solar in metal abundances, and equilibrium in collisional ionization. We also constrain the effective line-of-sight extent of the gas to be 3.4(1.0, 10.1) kpc, strongly suggesting that the enhancement most likely represents a Galactic central phenomenon.

Subject headings: Galaxy: structure — X-rays: ISM — X-rays: individual (3C 273, Mrk 421)

1. INTRODUCTION

The soft X-ray background (SXB) is greatly enhanced toward the inner part of the Galaxy ($l \lesssim 60°$), particularly obvious in the *ROSAT* All-Sky Survey (RASS) 3/4-keV band map (Fig. 1; Snowden et al. 1997). This Galactic central soft X-ray enhancement (GCSXE) apparently arises from diffuse hot gas; but its three-dimensional (3-D) morphology and origin are largely uncertain. The most prominent part of the GCSXE is along a ridge that is commonly considered to be associated with the North Polar Spur (NPS) — probably part of the radio continuum feature Loop I. The NPS is believed to be a local feature, based primarily on stellar polarization measurements (Bingham 1967); but this assertion is not universally accepted. The NPS and the rest of Loop I have been interpreted as a nearby ($D \sim 170$ pc) supernova remnant (SNR; e.g., Iwan 1980), a stellar wind bubble from the Scorpio-Centaurus OB association, or a combination of the two (e.g., Egger & Aschenbach 1995). Alternatively, the GCSXE could represent a recent outflow (e.g., a bipolar wind) or a giant explosion from the Galactic nuclear region (Sofue 1984; Bland-Hawthorn & Cohen 2003), or a more gentle but lasting Galactic bulge wind interacting with the Galactic gaseous halo (§ 4). In this case, the physical size of the enhancement must be comparable to our distance to the Galactic center ($\sim$ 8 kpc). Clearly, these scenarios have vastly different implications for the overall energetics of the GCSXE (i.e., 10^{51} vs. $\gtrsim 10^{54}$ ergs) and its impact on the global interstellar medium (ISM) structure of the Galaxy.

Studies of the GCSXE have been based primarily on broad-band X-ray observations such as the RASS (Snowden et al. 1997) and more recently on X-ray CCD observations from *XMM-Newton* and *Suzaku*. By observing the X-ray intensity variation on and off cool gas clouds at known distances, one can separate the foreground and background contributions (Burrows & Mendenhall 1991; Wang & Yu 1995; Park et al. 1997; Almy et al. 2000; Kuntz & Snowden 2000; Galeazzi et al. 2007; Smith et al. 2006; Henley et al. 2007). These experiments are particularly useful in isolating the local X-ray emission and hence determining the properties of hot gas in the solar neighborhood. However, to infer the properties of hot gas in distant regions is a much bigger challenge. Particularly uncertain is the correction for the absorption by intervening cool gas; the distribution of which relative to the X-ray-emitting hot gas can be a complex (e.g, Kuntz & Snowden 2000; Breitschwerdt & de Avillez 2006). Nevertheless, it has been shown that a large amounts of hot gas is present in regions toward the Galactic inner region and beyond $d \sim 2$ kpc (Almy et al. 2000). Along such a line of sight, one in general expects X-ray emission contributions from multiple components: the Local Hot Bubble (LHB; e.g., Snowden et al. 1998), the extended hot Galactic disk/corona (e.g., Yao & Wang 2005, 2007), the unresolved Galactic and extragalactic point sources (e.g., Kuntz & Snowden 2001; Hickox & Markevitch 2006), and the GCSXE. Of course, there could be additional discrete features such as the NPS, which is most likely a separate identity, independent of the GCSXE (see § 4). Direct spectral decomposition of these components along a single sight line is very difficult, if not impossible.

In this work, we present the first X-ray absorption line spectroscopy of the GCSXE, based on grating observations from the *Chandra X-Ray Observatory*. We compare the observations of 3C 273 and Mrk 421, on and off the GCSXE (Fig. 1) to determine its O VII and O VIII line absorptions. This differential spectroscopic data set enables us to characterize the

[1] Massachusetts Institute of Technology (MIT) Kavli Institute for Astrophysics and Space Research, 70 Vassar Street, Cambridge, MA 02139; yaoys@space.mit.edu
[2] Department of Astronomy, University of Massachusetts, Amherst, MA 01003; wqd@astro.umass.edu

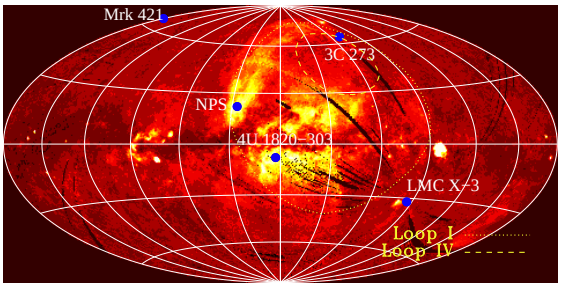

FIG. 1.— Directions of various relevant point sources (for X-ray absorption measurements) as well as the diffuse features: NPS and the radio loops I/IV (Haslam et al. 1971), shown on the RASS 3/4 keV band intensity map (Snowden et al. 1997) in Aitoff projection.

thermal and kinematic properties of the hot gas associated with the GCSXE with minimal uncertainties. The spectroscopic data, together with the emission intensity difference measured with the RASS, further allow us to estimate the effective path-length and density of the hot gas.

Throughout the paper, we quote the errors at the 90% confidence level, adopt the solar metal abundance from Anders & Grevese (1989), and assume that the hot gas is in the collisional ionization equilibrium (CIE) state and is approximately isothermal.

2. OBSERVATIONS AND DATA REDUCTION

As shown in Figure 1, the sight line of 3C 273 passes through the GCSXE, and is at the edges of radio loops I/IV. The 3/4-keV (RASS R4+R5 band) background is known to have quite a uniform intensity distribution, except for those abnormal regions such as the Galactic Bulge, NPS, the Cygnus Loop, etc. (Snowden et al. 1997). Much of the background emission in this band is proved to be thermal, with distinct line emission in high spectral resolution observations (McCammon et al. 2002). In contrast, the 1/4-keV (R1+R2 band) background intensity traces mostly hot gas in the LHB and residual emission from more distant regions after significant photo-electric absorption by foreground cool ISM. The background intensity in the 1/4-keV band appears patchy and shows little correlation with those in the higher energy bands. The background intensity in the 1.5-keV (R6+R7) band arises primarily from extragalactic AGNs. Therefore we only use the data in 3/4-keV band that are primarily due to O VII and O VIII line emission in the hot ISM (McCammon et al. 2002).

The diffuse 3/4-keV background intensity in the vicinity of the 3C 273 sight line is about 3 times of those at a typical high ($|b| \gtrsim 20°$) Galactic latitudes but away from the inner part of the Galaxy (e.g., Mrk 421 direction) and is about 1/5 of that at the brightest part of the NPS (Table 1; Snowden et al. 1997). We use Mrk 421 direction as a reference sight line, which has a Galactic latitude similar to the 3C 273 direction.

We use the RASS intensities in the R4 and R5 sub-bands to gain crude emission spectral characteristics of the 3C 273 and Mrk 421 sight lines. To account for the possible calibration uncertainties in the intensities of the individual energy bands, we add 10% [3] systematic uncertainty to the emission spectrum in our data analysis. To avoid the potential confusion from the emission of these bright sources due to the broad wing of the point spread function (PSF) of the RASS [4] and to smooth out any potential local emission gradient, we extract

[3] The calibration uncertainty in intensities of the individual bands is not available in the literature. The 10% is our attempted value.

[4] For a PSPC pointing observation with an off-axis of $0'(30')$, the PSF density at 0.5 keV drops $\sim 10^8(10^6)$ times at $\sim 1°$ away from the point source.

TABLE 1
PROPERTIES OF THE INTERESTED FIELDS

objects	(l, b)	$N_{\rm HI}$ ($\rm cm^{-2}$)	SXB Int.	Diffuse Int.
3C 273	(289.°95, 64.°36)	1.7×10^{20}	1.92×10^{-4}	1.29×10^{-4}
Mrk 421	(179.°83, 65.°03)	1.4×10^{20}	1.01×10^{-4}	0.39×10^{-4}
NPS	(26.°84, 21.°96)	5.6×10^{20}	7.58×10^{-4}	6.95×10^{-4}

NOTE. — The total HI absorption column density are adopted from Sembach et al. (2001) for 3C 273 and from Dickey & Lockman (1990) for Mrk 421 and NPS directions. The SXB intensities (in units of counts $\rm s^{-1}$ $\rm arcmin^{-2}$) toward 3C 273 and Mrk 421 are obtained from an annulus of 1.°0 to 1.°5 radii around the source on the 3/4-keV band RASS map. The diffuse intensities are obtained by subtracting the contributions from the unresolved extragalactic and Galactic point sources (§ 1). The intensities of the NPS (its brightest part) are obtained from a circular region of 1° radius.

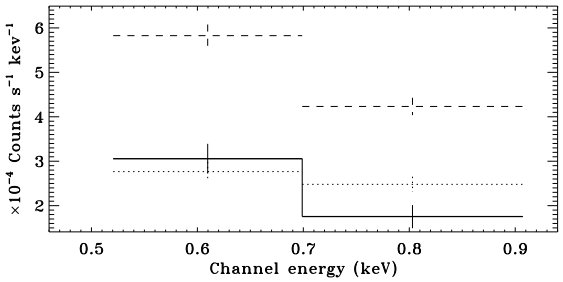

FIG. 2.— Spectrum of the emission associated with the GCSXE and in the direction of 3C 273 (*solid crosses*), the best-fit model convolved with the RASS response (*solid histogram*), and the SXB spectra toward 3C 273 (*dashed crosses*), and Mrk 421 (*dotted crosses*). See text for details.

the background intensities (Fig. 2) from an annulus of 1.°0 to 1.°5 radii centered at each of the sources, using the X-Ray Background Tool in HEASAC. [5]

The absorption spectra are extracted from an extensive set of *Chandra* grating observations, with an accumulated exposure time of $\sim$ 480 ks each for 3C 273 and Mrk 421. We have analyzed most of the observations of Mrk 421 in Yao & Wang (2007) and have detected significant O VII Kα, Kβ, and O VII Kα absorption lines in a co-added spectrum. For this study of the 3C 273 sight line, we use 13 observations taken with the Advanced CCD Imaging Spectrometer (ACIS). Among these observations (ObsID: 1198, 2464, 2471, 3574, 4431, 5170, 459, 2463, 3456, 3457, 3573, 4430, and 5169), the last seven used the High Energy Transmission Grating (HETG), for which only the data from the medium-energy-grating arms are included. We do not use two observations taken with the High Resolution Camera for a total exposure of $\sim$ 70 ks; their inclusion would increase the counting statistics only by $\sim$ 15% at $\sim$ 20 Å, but would also introduce the complex overlapping from high (> 1) order data (Yao & Wang 2006, 2007). We process the ACIS data, following the same procedure as described in Yao & Wang (2006, 2007).

We focus on the oxygen absorption lines to avoid the uncertainty in dealing with relative metal abundances. We fit the spectral continuum in the 18–22 Å range with a power law and fix the foreground cool gas absorption to be N_H^c = 1.7×10^{20} $\rm cm^{-2}$ (Sembach et al. 2001). This model fit gives χ^2/dof = 524/397; the strong O VII Kα, Kβ, and O VIII Kα

For Mrk 421 at its historical high flux ($\sim$ 50 times higher than the normal flux; e.g., the *Chandra* observation with ObsID 4148), the stray light from the point source contributes $\leq$ 0.2%(20%) to the SXB intensity of an annulus of 1.°0 to 1.°5 radii for R4+R5 band. The contribution from 3C 273 to the SXB intensity is negligible.

[5] http://heasarc.gsfc.nasa.gov/cgi-bin/Tools/xraybg/xraybg.pl

absorption lines are clearly visible in the residual. The inclusions of these absorption lines as described in § 3 significantly improves the fit ($\chi^2/\mathrm{dof} \simeq 402/392$). The resultant power-law index and the normalization are $2.1(2.0,2.3)$ and $2.3(2.2,2.5)\times10^{-2}$ photons keV^{-1} cm^{-2} s^{-1} at 1 keV.

The O VII Kα absorption line toward 3C 273 has already been detected by Fang et al. (2003), based on a subset of the observations used in this work. They have further discussed possible origins of the absorbing hot gas as a single component, either the intergalactic medium, the Galactic halo, or the radio loops I/IV. The detection of the additional absorption lines and the comparative analysis between the sight lines, as reported here, now make it possible to isolate and characterize the contribution from the GCSXE.

3. ANALYSIS AND RESULTS

We first characterize the absorbing gas by using our absline model[6] to jointly fit the O VII and O VIII absorption lines in the spectra of 3C 273 and Mrk 421. We measure the dispersion velocity (v_b), temperature (T), and the effective hydrogen column density ($N_{\rm H}$) of the gas along each sight line. Table 2 summarize the results, including the inferred O VI, O VII, and O VIII column densities. This single-temperature modeling represents only a simplified characterization of the gas. For example, a joint analysis of the emission and absorption data for Mrk 421 shows that the hot gas along the sight line is not isothermal (Yao & Wang 2007). We expect a more complicated temperature structure along the 3C 273 sight line. Nevertheless, the simple characterization, insensitive to the specific physical model adopted, should be sufficient for the modeling of averaged hot gas properties along the two sight lines, and thus facilitates a differential analysis of the GCSXE.

Comparing with the Mrk 421 sight line, the 3C 273 sight line is clearly affected by the hot gas associated with the GCSXE. The model characterizations of the two sight lines are substantially different, in terms of both thermal and kinematic properties as well as the total absorbing column densities (Table 2). We attribute this difference to the additional absorption produced by the GCSXE. We characterize this net GCSXE absorption by including a separate component in modeling the absorption along the 3C 273 sight line (Fig. 3). This component is in addition to the reference contribution assumed to be the same as that estimated from the Mrk 421 sight line (Table 2). Uncertainties in the reference contribution are neglected because the spectral signal-to-noise ratio of Mrk 421 (e.g., Fig. 1 in Yao & Wang 2007) is a factor of ~ 4.5 higher than that of 3C 273. The parameters of the GCSXE component are all free to be fitted.

Similarly, we subtract the emission spectrum toward Mrk 421 from that toward 3C 273 to obtain the net emission spectrum of the GCSXE (Fig. 2). We have ignored the small difference in the foreground cool gas absorptions between the two sight lines (Table 1). A correction for this difference will decrease the emission intensity toward Mrk 421 by $\lesssim$5%, which is much less than the statistical uncertainty (Fig. 2).

We measure the properties of the hot gas associated with the X-ray enhancement toward 3C 273 by jointly fitting the net emission and absorption spectra. This joint fit, as good as that for the absorption data alone, matches the emission spectrum well (Figs. 2-3). The fit gives v_b, T, and $N_{\rm H}$ and further allows us to infer $N_{\rm OVII}$, $N_{\rm OVIII}$, and $N_{\rm OVI}$ for the hot gas associated with the GCSXE (Table 2). The same fit also gives an estimate of the effective path-length through the gas as L = 3.4(1.0, 10.1) kpc. This inference uses the fact that the emission measure (EM) of the hot gas is proportional to its number density square ($EM \propto A_{\rm O} n_H^2 L\eta$), whereas the line absorption depends on the ionic column density ($N_H \propto N_{\rm OVII}/A_{\rm O} \propto n_H L\eta$). For simplicity, both the oxygen abundance $A_{\rm O}$ (in solar units) and the volume filling factor η are set to 1 in the quoted results (see § 4 for further discussions). Figure 4 shows the L versus T confidence contours. With these characterizations, we further infer the average density, pressure, and EM of the gas as $n_H = 2.1(0.4,6.6)\times10^{-3}$ cm^{-3}, $P/k = 4.22(0.8,13.3)\times10^3$ cm^{-3} K, and $EM = 1.9(0.6,6.3)\times10^{-2}$ cm^{-6} pc.

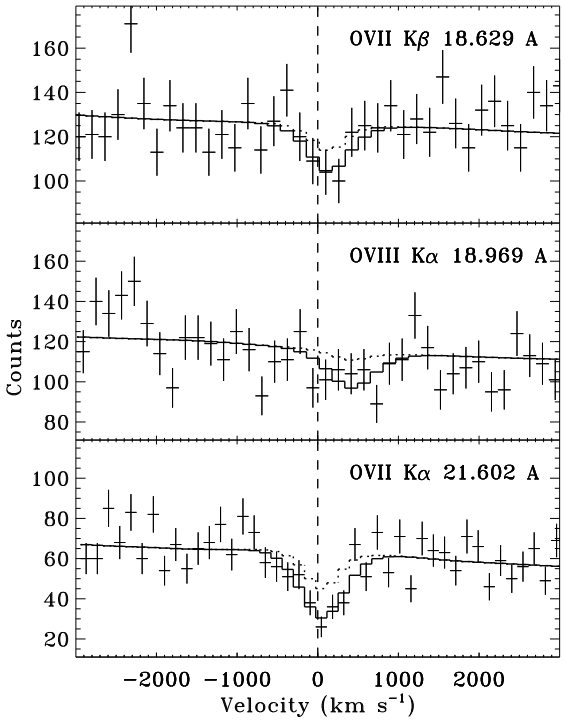

FIG. 3.— Detected oxygen absorption lines in the *Chandra* spectrum of 3C 273. The models have been convolved with the instrumental responses. The dotted histograms mark the amount of absorptions toward Mrk 421 direction. The bin size is 10 mÅ.

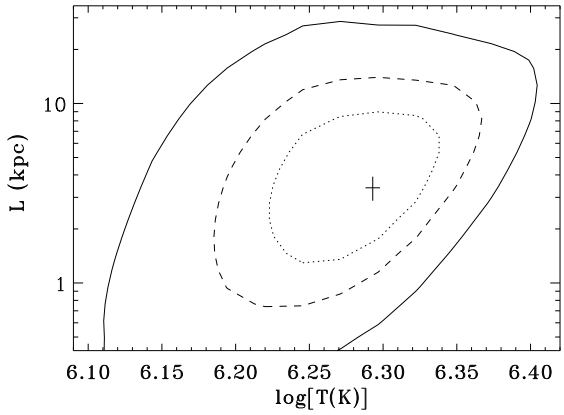

FIG. 4.— The 68%, 90%, and 99% confidence contours of the effective scale length (L) vs. the temperature (T) of the hot gas associated with the X-ray emission enhancement toward 3C 273.

[6] See Yao & Wang (2005) and Wang et al. (2005) for a detailed description of the model.

TABLE 2
SPECTRAL FIT RESULTS

direction	v_b (km s^{-1})	T (10^6 K)	N_H (10^{19} cm^{-2})	N_{OVII} (10^{16} cm^{-2})	N_{OVIII} (10^{15} cm^{-2})	N_{OVI} (10^{13} cm^{-2})
3C 273	139(92, 263)	1.7(1.4, 2.0)	3.5(2.3, 5.6)	2.0(1.3, 3.6)	8.0(3.1, 14.7)	6.0(3.8, 11.0)
Mrk 421	64(48, 104)	1.4(1.3, 1.6)	1.4(1.0, 2.0)	1.0(0.7, 1.5)	1.5(0.6, 2.6)	3.2(2.1, 5.0)
GCSXE[a]	216(104, 480)	2.0(1.6, 2.3)	2.2(1.4, 4.1)	1.0(0.6, 2.6)	7.2(2.0, 13.3)	3.2(1.8, 8.2)

NOTE. — In our absorption line model, the transition oscillation coefficient and the damping factor are adopted from Verner et al. (1996) for O VII and O VIII, and from Morton (2003) for O VI. 90% confidence intervals given in parenthesis.
[a] The GCSXE contribution along the sight line toward 3C 273 direction. See text for the details.

4. DISCUSSION

We have obtained the dispersion velocity, temperature, absorption column density, and the effective path-length of the diffuse gas associated with the X-ray emission enhancement toward the 3C 273 direction. The 90% lower limit of the path-length, $L \gtrsim 1$ kpc, places the gas well beyond any possible local origin within a distance of $D \lesssim 200$ kpc, and therefore favors a remote origin of the gas. The emission enhancement most likely reflects an outflow from the Galactic center (GC) and/or bulge region. Large-scale winds driven by galactic nuclear starbursts and/or AGNs have been observed in many galaxies (e.g., Martin 1999; Heckman et al. 2001). In our Galaxy, there is also evidence for the powerful energy injection from the GC on scales of several arcminutes to tens of degrees from radio to γ-ray (see Morris & Serabyn 1996; Veilleux et al. 2005 for reviews). The outflow is also expected from the energy and mass injection from the Galactic bulge due to Type Ia supernovae and ejection of evolving low-mass stars. In any case, the outer boundary of the GCSXE may represent the interaction region of such an outflow with the Galactic disk and the accretion from the intergalactic medium (Wang 2007).

The large velocity dispersion ($v_b \sim 216$ km s^{-1}) of the gas along the 3C 273 sight line supports the GC origin of the GCSXE (Table 2). Our estimate of the dispersion is based essentially on the relative saturation of the observed O VII Kα and Kβ absorption lines and is consistent with the presence of an O VI high velocity absorption wing (extending up to ~ 240 km s^{-1}), detected in the *FUSE* spectrum of 3C 273 (Sembach et al. 2001). The dispersion is significantly higher than those estimated for the Mrk 421 sight line and for a similar off-GCSXE direction toward LMC X–3 (Galactic coordinates $l, b = 273.^\circ57, -32.^\circ08$; Fig. 1; Wang et al. 2005), indicating different natures of the intervening media. At a temperature of $\sim 2 \times 10^6$ K, the thermal broadening for the O VII-bearing gas is ~ 45 km s^{-1}, which is negligible compared to v_b, indicating a large nonthermal broadening. This broadening cannot be due to the differential rotation of the Galactic disk, because of the high Galactic latitude direction and is most likely due to the very turbulent nature of the gas, as is expected in the interaction region.

It is also instructive to compare properties of the hot gas associated with the emission enhancement in the sight line of 3C 273 with those of the LHB. The temperature of the LHB is commonly accepted to be $\sim 10^6$ K, but the EM is still poorly constrained, ranging from 0.0079 to 0.02 cm^{-6} pc (e.g., Smith et al. 2006; Galeazzi et al. 2007; Henley et al. 2007). Taking an average size of the LHB as 100 pc (e.g., Sfeir et al. 1999), the EM implies an absorbing column density of $2.7-4.4 \times 10^{18}$ cm^{-2} across the LHB. The obtained column density of the hot gas associated with the enhancement, $\sim 2.2 \times 10^{19}$ cm^{-2} (Table 2), can therefore accommodate $\sim$ 5-7 bubble boundaries like those of the LHB in the line of sight, implying a size of the hot gas $\gtrsim 500$ pc. The temperature of the hot gas is ~ 2 times higher than that of the LHB (Table 2). Therefore, if the thermal pressure could be assumed to be roughly the same as that in the LHB, the size of the GCSXE would then be larger. This simple comparison also suggests that the GCSXE represents a remote phenomenon.

How does the conclusion depend on our assumed solar metal abundances of the hot gas? We have used only the X-ray absorption lines produced by oxygen ions. For a plasma at $\sim 2 \times 10^6$ K, O VII and O VIII dominates ($\geq 85\%$) the emission in the RASS 3/4-keV band. Therefore, a deviation of non-oxygen metal elemental abundances from the assumed solar values will not significantly change our L estimate. For example, assuming the abundances equal to zero would give $L = 2.8(0.9, 9.1)$ kpc, whereas adopting the abundances to be supers-solar would lead to a slightly larger L. The L is nearly inversely proportional to the oxygen abundance. To let the GCSXE be consistent with a local origin (i.e., $L \lesssim 200$ pc; § 1) the oxygen abundance needs to be $\gtrsim 5$ (90% lower limit; § 3) times solar, which is very unlikely.

With the characterizations of the hot gas obtained in § 3, we can estimate the thermal energy contained in wind material. We take a simple bipolar glass-timer geometry for the wind with a cone-like shape near the GC and a cylindric shape at large vertical distances ($5 \leq |z| \leq 20$ kpc; e.g., Sofue 2000; Bland-Hawthorn & Cohen 2003). The radius of the cylinder is assumed to be ~ 7.2 kpc, to be consistent with our estimated path-length ($L \sim 3.4$ kpc) along the 3C 273 sight line (taking the distance to the Galactic center of 7.6 kpc; Eisenhauer et al. 2005). To simplify our calculation, we assume that the gas density is uniformly distributed and the gas temperature is exponentially decaying along the vertical direction from 5×10^6 K near the GC (e.g., Park et al. 1997) to 2×10^6 K at the latitude of 3C 273 (Table 2). We find that total energy is $\sim 10^{56}$ ergs, which is roughly in line with that expected in the GC wind models (Sofue 2000; Bland-Hawthorn & Cohen 2003).

While the emission enhancement toward 3C 273 likely arises in a region around the GC, the bright NPS may still have a local origin (e.g., de Geus 1992). In this case, the NPS may be superposed on the large-scale GCSXE, which appears much more extended (to regions with $l \gtrsim 60^\circ$; Fig. 1). Miller et al. (2006) recently presented a high resolution *Suzaku* emission spectrum of the bright NPS (Table 1). From a multiple component fit, they found that while the relative abundances of Ne/O, Fe/O, and Mg/O are consistent with the solar values, the N/O is ~ 4 times higher. They therefore attributed the NPS to the Sco-Cen environment, being enriched by material undergoing the CNO cycle in massive stars. In addition, the temperature they obtained,

$\sim 3.4 \times 10^6$ K, is substantially higher than that of the GCSXE, as we have obtained here (Table 2). A similarly high temperature was also obtained from the *XMM-Newton* observations (Willingale et al. 2003). The apparent high temperature of the NPS may be due to the high-velocity shock-heating, commonly seen in young supernova remnants.

We have assumed that the hot gas associated with the GCSXE along the 3C 273 sight line is isothermal, which is adequate in the present study due to the very limited spectral resolution of the RASS data used here. Emission data with a low instrument background and relatively high spectral resolution (e.g., from a deep *Suzaku* X-ray CCD observation) will be particularly useful for tightening the constraints on the properties of the hot gas associated with the GCSXE.

We thank Eric Miller, Claude Canizares, Paola Testa, and Herman Marshall for useful discussions. We are also grateful to the anonymous referee for insightful comments and suggestions, which helped to improve the presentation of the paper. This work is supported by NASA through the Smithsonian Astrophysical Observatory contract SV3-73016 to MIT for support of the *Chandra* X-Ray Center under contract NAS 08-03060. Support from *Chandra* archival research grant AR7-8016 are also acknowledged. QDW appreciates additional support from NASA grant NNX06AB99G.

REFERENCES

Almy, R. C., McCammon, D., Digel, S. W., et al. 2000, ApJ, 545, 290
Anders, E., & Grevesse, N. 1989, Geochim. Cosmochim. Acta, 53, 197
Bingham, R. G. 1967, MNRAS, 137, 157
Bland-Hawthorn, J., & Cohen, M. 2003, ApJ, 582, 246
Breitschwerdt, D., & de Avillez, M. A. 2006, A&A, 452L, 1
Burrows, D. N., & Mendenhall, J. A. 1991, Nature, 351, 629
de Geus, E. J. 1992, A&A, 262, 258
Dickey, J. M., & Lockman, F. J. 1990, ARA&A, 28, 215
Egger, R. J., & Aschenbach, B. 1995, A&A, 294, L25
Eisenhauer, F., Genzel, R., Alexander, T., et al. 2005, ApJ, 628, 246
Heckman, T. M., Sembach, K. R., Meurer, G. R., et al. 2001, ApJ, 554, 1021
Henley, D. B., Shelton, R. L., & Kuntz, K. D. ApJ 661, 304
Fang, T., Sembach, K., & Canizares, C. 2003, ApJ, 586, L49
Galeazzi, M., Gupta, A., Covey, K., & Ursino, E. 2007, ApJ, 658, 1081
Haslam, C. G. T., Kahn, F. D., & Meaburn, J. 1971, A&A, 12, 388
Hickox, R., & Markevitch, M. 2006, ApJ, 645, 95
Iwan, D. 1980, ApJ, 239, 316
Kuntz, K. D., & Snowden, S. L. 2000, ApJ, 543, 195
——. 2001, ApJ, 554, 684
Martin, C. L. 1999, ApJ, 513, 156
McCammon, D., Almy, R., Apodaca, E., et al. 2002, ApJ, 576, 188
Miller, E., Tsunemi, H., Bautz, M., et al. 2006, AAS, 208, 3504
Morris, M., & Serabyn E. 1996, ARA&A, 34, 645
Morton, D. C. 2003, ApJS, 149, 205
Park, S., Finley, J. P., Snowden, S. L., & Dame, T. M. 1997, ApJ, 476, L77
Sembach, K. R., Howk, J. C., Savage, B. D., Shull, et al. 2001, ApJ, 561, 573
Sfeir, D. M., Lallement, R., Crifo, F., & Welsh, B. Y. 1999, A&A, 346, 785
Smith, R. K., et al. 2006, PASJ 59, 141
Snowden, S. L., et al. 1997, ApJ, 485. 125
——. 1998, ApJ, 493, 715
Sofue, Y. 1984, Nature, 310, 568
——. 2000, ApJ, 540, 224
Veilleux, S., Cecil, G., & Bland-Hawthorn 2005, ARA&A, 43, 769
Verner, D, A., Verner, E. M., & Ferland, G. J. 1996, Atomic Data & Nuclear Data Tables, 64, 1-180
Wang, Q. D. & Yu, K. 1995, AJ, 102, 698
Wang, Q. D., Yao, Y., Tripp, T. M., et al. 2005, ApJ, 635, 386
Wang, Q. D. in the proceedings of Chemodynamics: from first stars to local galaxies, in press (astro-ph/0611038)
Willingale, R., Hands, A. D. P., Warwick, R. S., et al. 2003, MNRAS, 343, 995
Yao, Y., & Wang, Q. D. 2005, ApJ, 624, 751
——. 2006, ApJ, 641, 930
——. 2007, ApJ, 658, 1088